Title: RANS modeling of RTI and HVDT with BHR3

Author(s):   Trettel, Ben

Intended for: arXiv
                 Report
                 Web

RANS modeling of RTI and HVDT with BHR3

Ben Trettel[1]   August 15, 2012

Abstract

The BHR3 turbulence model was improved to include two different scales as suggested by Livescu et al. [Liv+09, §4.4.6]: one for turbulent transport and the other for turbulent dissipation. Additionally, destruction terms modeled analogously to production terms were added to the turbulent mass-weighted velocity equation. New model coefficients were developed for this model. The first change was to use $C_2 = 1.77$ for the isotropic turbulence decay coefficient rather than the k-ϵ model's 1.92, which is outside of the experimentally measured values [ML90; KF09].

The new model coefficients were developed to accurately model a wide range of experimental and numerical results: constant and variable density Kelvin-Helmholtz instabilities, Rayleigh-Taylor instabilities, and homogeneous variable density turbulence (HVDT) [LR07]. My work focused on the buoyancy-driven flows: Rayleigh-Taylor instabilities and HVDT.

1 Rayleigh-Taylor instability background

A Rayleigh-Taylor instability occurs when a light fluid is under a heavy fluid. If a force is applied that leads to an acceleration, the fluids will start to mix. Small disturbances (e.g. density fluctuations as shown in figure 1) that are always present in real flows will initiate the Rayleigh-Taylor instability. This instability eventually goes turbulent as can be seen in figure 2.
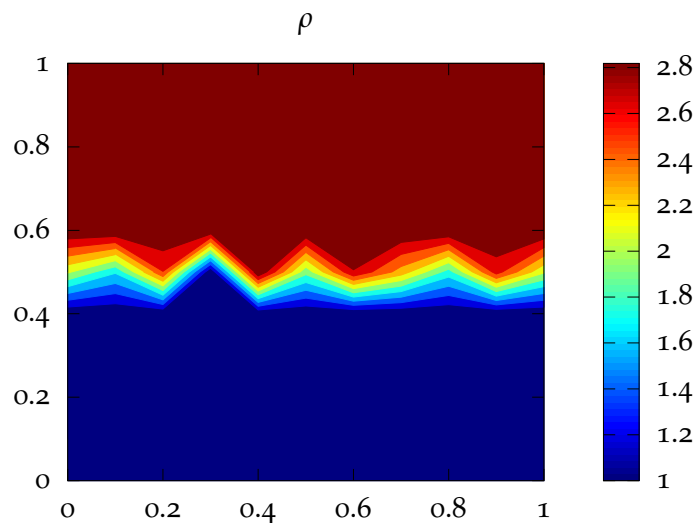
Figure 1: Initial conditions of a hypothetical Rayleigh-Taylor instability.

Figure 2 shows a spatially developing mixing layer, i.e., the two fluids start on the right separated by a splitter plate but flow to the left, leaving the splitter place, which allows them to mix while moving. Each vertical slice of fluid mixes as they move. This configuration is statistically steady — the time-averaged solution is steady.

The simulations described in this work develop temporally. A heavy fluid is placed above a lighter fluid, and the two fluids mix in time.

The Rayleigh-Taylor instability is controlled by the mass density difference of the two fluids. This density

1   Dept. of Fire Protection Engineering, University of Maryland, College Park. Email: ben.trettel@gmail.com

Figure 2: View of a spatially developing Rayleigh-Taylor instability from experiments by Banerjee, Kraft, and Andrews [BKA10, p. 133] for A = 0.47. The white fluid is lighter than the dark fluid. The fluids are moving to the left at 1.65 m/s.

difference is non-dimensionalized to form the Atwood number, defined as

$$A = \frac{\rho_H - \rho_L}{\rho_H + \rho_L} \,, \tag{1.1}$$

where ρ_H is the density of the heavy fluid and ρ_L is the density of the lighter fluid.

A key quantity of interest in the Rayleigh-Taylor instability is the width of the mixing layer and how fast it grows. For large times, this width can be shown to be [BKA10, p. 128]

$$h(t) = \alpha \, A \, g t^2 \tag{1.2}$$

where α is the growth rate, g is the gravitational acceleration due to gravity, and t is time.

Drazin and Reid [DR04] detail the theory behind a variety of different hydrodynamic instabilities, including for Rayleigh-Taylor instabilities.

2 Model description and development

The equations governing the flow of single-phase mixtures of compressible fluids are [Sch+11; PV05]

$$\frac{\partial \rho}{\partial t} + \frac{\partial}{\partial x_j} \left(\rho u_j \right) = 0 \,, \tag{2.1}$$

$$\frac{\partial \rho u_i}{\partial t} + \frac{\partial}{\partial x_j} \left(\rho u_i u_j + P \delta_{ij} \right) = \frac{\partial \tau_{ij}}{\partial x_j} + \rho g_i \,, \tag{2.2}$$

$$\frac{\partial \rho E}{\partial t} + \frac{\partial}{\partial x_j} \left(\rho u_j E + P u_j \right) = \frac{\partial}{\partial x_j} \left(\tau_{ij} u_i - q_i \right) \,, \tag{2.3}$$

$$\frac{\partial \rho c_n}{\partial t} + \frac{\partial}{\partial x_j} \left(\rho (u_j + V_{n,j}) c_n \right) = 0 \,. \tag{2.4}$$

where

ρ is the mass density,

u_j is the j-th component of the fluid velocity,

P is the thermodynamic pressure,

τ is the shear stress tensor,

g_i is the acceleration due to gravity in the i-th direction,

E is the total energy (sensible and kinetic — see Poinsot and Veynante [PV05, p. 21]) per unit mass,

q_i is the total heat flux,

c_n is the mass fraction for species n, and

$V_{n,j}$ is the j-th component of the diffusion velocity.

To fully close this system additional equations are needed including equations of state for thermodynamic pressure and internal energy and equations modeling the viscous stress, heat flux, and mass diffusion.

For Reynolds averaging, quantities are decomposed into mean ($\bar{u}$) and fluctuating (u') components [Pop00, p. 83]:

$$u = \bar{u} + u' . \tag{2.5}$$

The type of averaging used includes time, space, and ensemble averaging. Pope [Pop00, ch. 3] details the definitions of these statistics among others.

For variable-density and compressible flows, mass weighted averages called Favre averages are preferred to avoid additional unclosed terms that need to be modeled. A Favre averaged quantity is defined as

$$\widetilde{u} \equiv \frac{\overline{\rho u}}{\bar{\rho}} \tag{2.6}$$

and the quantity u is split into mean and fluctuating components

$$u = \widetilde{u} + u'' . \tag{2.7}$$

After averaging the fluid equations are Schwarzkopf et al. [Sch+11, sec. 2]

$$\frac{\partial \bar{\rho}}{\partial t} + \frac{\partial}{\partial x_j} \left(\bar{\rho} \widetilde{u}_j \right) = 0 , \tag{2.8}$$

$$\frac{\partial}{\partial t} \left(\bar{\rho} \widetilde{u}_i \right) + \frac{\partial}{\partial x_j} \left(\bar{\rho} \widetilde{u}_i \widetilde{u}_j + \overline{P} \delta_{ij} + \bar{\rho} \widetilde{R}_{ij} \right) = \bar{\rho} g_i , \tag{2.9}$$

$$\frac{\partial}{\partial t} \left(\bar{\rho} \widetilde{E} \right) + \frac{\partial}{\partial x_j} \left(\bar{\rho} \widetilde{u}_j \widetilde{E} \right) = -\frac{\partial}{\partial x_j} \left(\overline{P} \widetilde{u}_j \right) - \frac{\partial}{\partial x_j} \left(\bar{\rho} \widetilde{u}_i \widetilde{R}_{ij} \right) - \frac{\partial}{\partial x_j} \left(\overline{P' u'_j} \right)$$
$$- \frac{\partial}{\partial x_j} \left(\overline{\rho E'' u''_j} \right) - \frac{1}{2} \frac{\partial}{\partial x_j} \left(\overline{\rho u''_i u''_i u''_j} \right) - \frac{\partial \bar{q}_j}{\partial x_j} , \tag{2.10}$$

$$\frac{\partial}{\partial t} \left(\bar{\rho} \widetilde{c}_n \right) + \frac{\partial}{\partial x_j} \left(\bar{\rho} \widetilde{u}_j \widetilde{c}_n \right) = -\frac{\partial}{\partial x_k} \left(\overline{\rho u''_k c''_n} \right) \tag{2.11}$$

where $\widetilde{R}_{ij} \equiv \overline{\rho u''_i u''_j} / \bar{\rho}$ are the components of the Favre averaged Reynolds stress tensor. The equations have many "unclosed terms" that must be modeled including the Reynolds stress. The BHR3 model closes these equations.

3

A derivation of the Reynolds stress transport equation for single-phase compressible flows can be found in Cebeci and Smith [CS74, Ch. 2].

2.1 BHR3 model development

Schwarzkopf et al. [Sch+11, sec. 3] reviews the development of the single scale version of the BHR3 turbulence model. The primary changes since that work are the inclusion of two turbulence scales (one for turbulent transport and the other for turbulent dissipation) as opposed to one and adding destruction terms modeled analogously to production terms in the turbulent mass-weighted velocity (a_i) equation.

The use of two scales is motivated by turbulence's multiscale physics. The energy spectrum of turbulence [Pop00, ch. 6] includes many scales ranging from the scales of the dimensions of the domain studied down to the smallest scales of the flow, the Kolmogorov scales. The smallest length scales dissipate energy under the "energy cascade" viewpoint that Pope describes. Turbulent transport is associated with the larger physical scales as the geometry usually dictates the resolved (i.e., large scale) transport.

Additionally, Livescu et al. [Liv+09, §4.4.6] describes why buoyancy-driven flows have at least two distinct length scales. To summarize, the increase in energy of the large scales from buoyancy takes time to be felt by the dissipation scales. Thus, at least these two distinct scales are necessary to accurately model buoyancy-driven flows.

The BHR3 model includes two quantities to model the mixing: the density-specific-volume covariance, $b \equiv -\overline{\rho'(1/\rho)'}$, and the turbulent mass-weighted velocity, $a_i \equiv -\overline{u''} = \overline{\rho' u_i'}/\overline{\rho}$. The density-specific-volume covariance is a measure of the mixing. In a fully mixed region b is zero. The turbulent mass-weighted velocity represents the coupling of density and velocity and is zero for single-phase incompressible flows. The turbulent mass-weighted velocity is also related to the turbulent mass flux, $\overline{\rho}a_i$.

The new model for destruction of a_i is simple — the production and destruction of a_i are related and an "effective" production can be found by simply assuming that some of the destruction of a_i is proportional to the production of a_i.

The next few sections list the full BHR3 equations. Descriptions of several terms are underbraced.

2.2 Length and time scales

$$
\frac{\partial \overline{\rho} S_{\text{diff}}}{\partial t} + \frac{\partial}{\partial x_j}\left(\overline{\rho}\widetilde{u}_j S_{\text{diff}}\right) = \underbrace{-\frac{S_{\text{diff}}}{K}\left(\frac{3}{2}-C_1\right)\overline{\rho}\widetilde{R}_{ij}\frac{\partial \widetilde{u}_i}{\partial x_j} - \left(\frac{3}{2}-C_2\right)\overline{\rho}\sqrt{K} + \frac{S_{\text{diff}}}{K}\left(\frac{3}{2}-C_4\right)a_j\frac{\partial \overline{P}}{\partial x_j} - C_3\overline{\rho}S_{\text{diff}}\frac{\partial \widetilde{u}_j}{\partial x_j}}_{\text{net production}}
$$

$$
\underbrace{+C_s\frac{\partial}{\partial x_k}\left(\frac{S_{\text{diff}}}{\sqrt{K}}\overline{\rho}\widetilde{R}_{kn}\frac{\partial S_{\text{diff}}}{\partial x_n}\right)}_{\text{diffusion}} \tag{2.12}
$$

$$
\frac{\partial \overline{\rho} S_{\text{diss}}}{\partial t} + \frac{\partial}{\partial x_j}\left(\overline{\rho}\widetilde{u}_j S_{\text{diss}}\right) = \underbrace{-\frac{S_{\text{diss}}}{K}\left(\frac{3}{2}-C_{1v}\right)\overline{\rho}\widetilde{R}_{ij}\frac{\partial \widetilde{u}_i}{\partial x_j} - \left(\frac{3}{2}-C_{2v}\right)\overline{\rho}\sqrt{K} + \frac{S_{\text{diss}}}{K}\left(\frac{3}{2}-C_{4v}\right)a_j\frac{\partial \overline{P}}{\partial x_j} - C_{3v}\overline{\rho}S_{\text{diss}}\frac{\partial \widetilde{u}_j}{\partial x_j}}_{\text{net production}}
$$

$$
\underbrace{+C_s\frac{\partial}{\partial x_k}\left(\frac{S_{\text{diss}}}{\sqrt{K}}\overline{\rho}\widetilde{R}_{kn}\frac{\partial S_{\text{diss}}}{\partial x_n}\right)}_{\text{diffusion}} \tag{2.13}
$$

$$
\tau_{\text{diss}} \equiv \frac{S_{\text{diss}}}{\sqrt{K}} \quad , \quad \tau_{\text{diff}} \equiv \frac{S_{\text{diff}}}{\sqrt{K}} \tag{2.14}
$$

4

2.3 Reynolds stress

$$\frac{\partial \left(\overline{\rho}\widetilde{R}_{ij}\right)}{\partial t} + \frac{\partial}{\partial x_k}\left(\overline{\rho}\widetilde{u}_k\widetilde{R}_{ij}\right) = \underbrace{a_i\frac{\partial \overline{P}}{\partial x_j} + a_j\frac{\partial \overline{P}}{\partial x_i} - \overline{\rho}\widetilde{R}_{ik}\frac{\partial \widetilde{u}_j}{\partial x_k} - \overline{\rho}\widetilde{R}_{jk}\frac{\partial \widetilde{u}_i}{\partial x_k}}_{\text{net production}} + \underbrace{C_{r3}\frac{\partial}{\partial x_k}\left(\tau_{\text{diff}}\overline{\rho}\widetilde{R}_{km}\frac{\partial \widetilde{R}_{ij}}{\partial x_m}\right)}_{\text{diffusion}} - \underbrace{\overline{\rho}\frac{2}{3}\frac{K}{\tau_{\text{diss}}}\delta_{ij}}_{\text{destruction}}$$

$$+ \underbrace{\overline{\rho}C_{r2}\left(\widetilde{R}_{ik}\frac{\partial \widetilde{u}_j}{\partial x_k} + \widetilde{R}_{jk}\frac{\partial \widetilde{u}_i}{\partial x_k}\right) - C_{r2}\frac{2}{3}\overline{\rho}\widetilde{R}_{mk}\frac{\partial \widetilde{u}_m}{\partial x_k}\delta_{ij} - C_{r1}\left(a_i\frac{\partial \overline{P}}{\partial x_j} + a_j\frac{\partial \overline{P}}{\partial x_i}\right) + C_{r1}\frac{2}{3}a_k\frac{\partial \overline{P}}{\partial x_k}\delta_{ij}}_{\text{rapid return to isotropy}}$$

$$+ \underbrace{C_{r4}\overline{\rho}\frac{1}{\tau_{\text{diss}}}\left(\widetilde{R}_{ij} - \frac{1}{3}\widetilde{R}_{kk}\delta_{ij}\right)}_{\text{slow return to isotropy}} \tag{2.15}$$

2.4 Turbulent mass-weighted velocity

$$\frac{\partial \overline{\rho}a_i}{\partial t} + \frac{\partial}{\partial x_k}\left(\overline{\rho}\widetilde{u}_k a_i\right) = \underbrace{(1 - C_{\text{ap}})b\frac{\partial \overline{P}}{\partial x_i} - (1 - C_{\text{ar}})\widetilde{R}_{ik}\frac{\partial \overline{\rho}}{\partial x_k} - (1 - C_{\text{au}})\overline{\rho}a_k\frac{\partial \widetilde{u}_i}{\partial x_k}}_{\text{net production}} + \underbrace{\overline{\rho}\frac{\partial}{\partial x_k}\left(a_k a_i\right)}_{\text{redistribution}}$$

$$+ \underbrace{\overline{\rho}C_a\frac{\partial}{\partial x_k}\left(\tau_{\text{diff}}\widetilde{R}_{kn}\frac{\partial a_i}{\partial x_n}\right)}_{\text{diffusion}} - \underbrace{C_{a1}\overline{\rho}\frac{1}{\tau_{\text{diss}}}a_i}_{\text{destruction}} \tag{2.16}$$

2.5 Density-specific-volume covariance

$$\frac{\partial \overline{\rho}b}{\partial t} + \frac{\partial}{\partial x_k}\left(\overline{\rho}b\widetilde{u}_k\right) = \underbrace{-2(b+1)a_k\frac{\partial \overline{\rho}}{\partial x_k}}_{\text{production}} + \underbrace{2\rho a_k\frac{\partial b}{\partial x_k}}_{\text{redistribution}} + \underbrace{\overline{\rho}^2 C_b\frac{\partial}{\partial x_k}\left(\frac{\tau_{\text{diff}}}{\overline{\rho}}\widetilde{R}_{kn}\frac{\partial b}{\partial x_n}\right)}_{\text{diffusion}} - \underbrace{C_{b1}\overline{\rho}\frac{1}{\tau_{\text{diss}}}b}_{\text{destruction}} \tag{2.17}$$

2.6 Species mass fraction

$$\frac{\partial \overline{\rho}\widetilde{c}_n}{\partial t} + \frac{\partial}{\partial x_j}\left(\overline{\rho}\widetilde{c}_n\widetilde{u}_j\right) = \frac{\partial}{\partial x_k}\left(C_c\frac{S_{\text{diff}}}{\sqrt{K}}\overline{\rho}\widetilde{R}_{km}\frac{\partial \widetilde{c}_n}{\partial x_m}\right) \tag{2.18}$$

3 Modeling the Rayleigh-Taylor instability

LANL's code Rage [Git+08] was used to model Rayleigh-Taylor instabilities. The Atwood number used for these simulations was 0.5 and the results were compared against DNS data by Cabot and Cook [CC06] that was processed by Livescu et al. [Liv+09] and experiments by Banerjee, Kraft, and Andrews [BKA10].

3.1 Non-dimensionalization

The z location in the Rayleigh-Taylor mixing layer was non-dimensionalized by an integral mix width defined by [AS90]

$$h(t) \equiv 6\int_{-\infty}^{\infty} f_v(1 - f_v)dz \quad , \quad f_v \equiv \frac{\rho - \rho_L}{\rho_H - \rho L} . \tag{3.1}$$

case	DNS growth rate	exp. growth rate	RANS growth rate
Rayleigh-Taylor ($A = 0.5$)	0.0416	0.141	0.0447
Kelvin-Helmholtz	0.062	0.069	0.067

Table 1: Growth rates for the Rayleigh-Taylor ($A = 0.5$) case and Kelvin-Helmholtz case for comparison. The RT DNS growth rate is from the data-set of Cabot and Cook [CC06] and the experimental growth rate is from Banerjee, Kraft, and Andrews [BKA10, p. 153] where the total growth rate is the sum of the two integral half mix-widths interpolated for $A = 0.5$. For KH, the DNS growth rate is from Rogers and Moser [RM94], the experimental growth rate is from Bell and Mehta [BM90], and the RANS BHR3 growth rate is from Smith [Smi12, §3.1].

The times were non-dimensionalized by [Sch+11, p. 25]

$$\tau \equiv \sqrt{\frac{h(t)}{A\,|g|}}\ , \tag{3.2}$$

the velocities by

$$\lambda \equiv \frac{h(t)}{\tau}\ , \tag{3.3}$$

and the energies by λ^2.

3.2 Quantifying the model's fit

I wanted a fast and easy way to approximately quantify how well the output from a run fit experimental or DNS data. I developed a metric that my post-processing script (which is in an appendix) could output. This metric was the sum of the errors in K, b, and a_z of the peak values, integral, width (where, as detailed before, the ideal width is 1), and growth rate. The RANS model was compared solely against the DNS data due to the discrepancy in the growth rates between the experiments and DNS. The DNS data was smoothed a bit to reduce the effects of some small fluctuations in it that can not be represented in the RANS simulation.

The BHR3 model does not accurately predict the tails of the Rayleigh-Taylor instability as can be seen in figures 3 through 5. The tails of the RANS data are sharper than the tails of the DNS data. This problem occurs because the tails of the DNS Rayleigh-Taylor layer are not fully turbulent. BHR3 applies to the turbulent center of mixing layer, not the edges [Liv12]. Thus, BHR3 is not capable of complete accuracy in the tails. In the tails, the instability retains memory of the initial conditions, which affects the growth rate of the tails as explained below.

3.3 Growth rate

The growth rate of the Rayleigh-Taylor instability is only found in the self-similar regime, where the previously detailed non-dimensionalization collapses all times into a single curve.

The growth rate was calculated with the following formula:

$$\alpha = \left(\frac{\sqrt{h(t)} - \sqrt{h(t_0)}}{\sqrt{A\,g}\,(t - t_0)} \right)^2 \tag{3.4}$$

as Schwarzkopf et al. [Sch+11, p. 22] did.

The growth rate for the Rayleigh-Taylor experiments is found to be over 3 times as high as the DNS

growth rate as seen in table 1. Livescu [Liv12] attributes the difference in the growth rates between the experiments and simulations to the effects of the initial and boundary conditions. Low-wavenumber oscillations that exist in reality influence the growth rates. Because of the difficulty in prescribing initial and boundary conditions, the RANS growth rate was matched to the DNS growth rate in this work.

3.4 Results

For the model coefficients developed in this work, plots of turbulent kinetic energy (K), density-specific-volume covariance (b), and turbulent mass-weighted velocity (a_z) are plotted in figures 3 through 5. Unlike in previous work [Sch+11], the fit of the BHR3 model and the DNS is excellent.
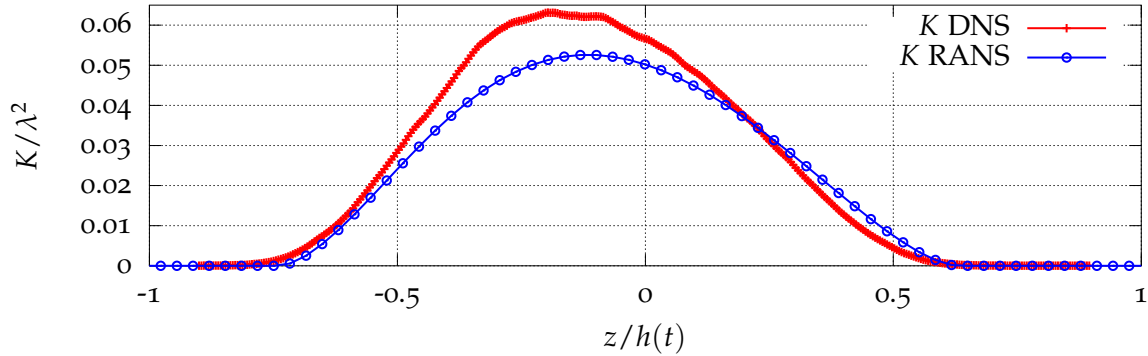

Figure 3: Comparison of DNS and RANS results for the turbulent kinetic energy, K, for A = 0.5.
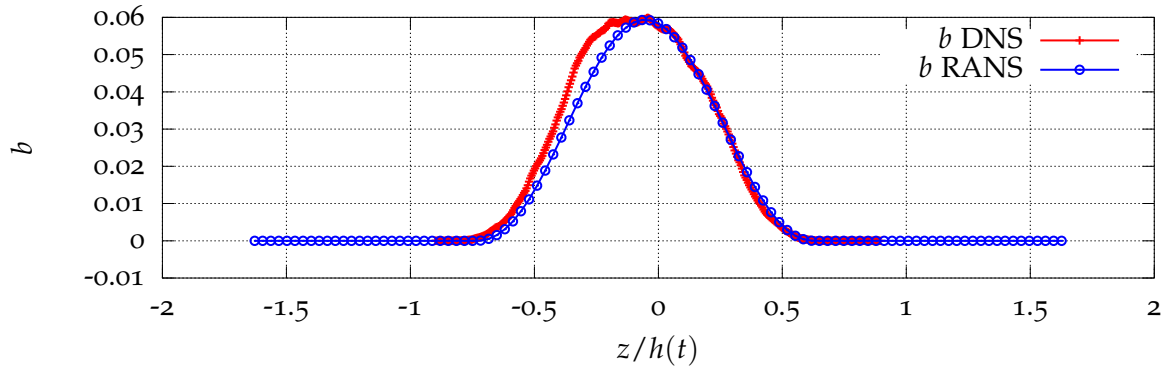

Figure 4: Comparison of DNS and RANS results for the density-specific-volume covariance, b, for A = 0.5.
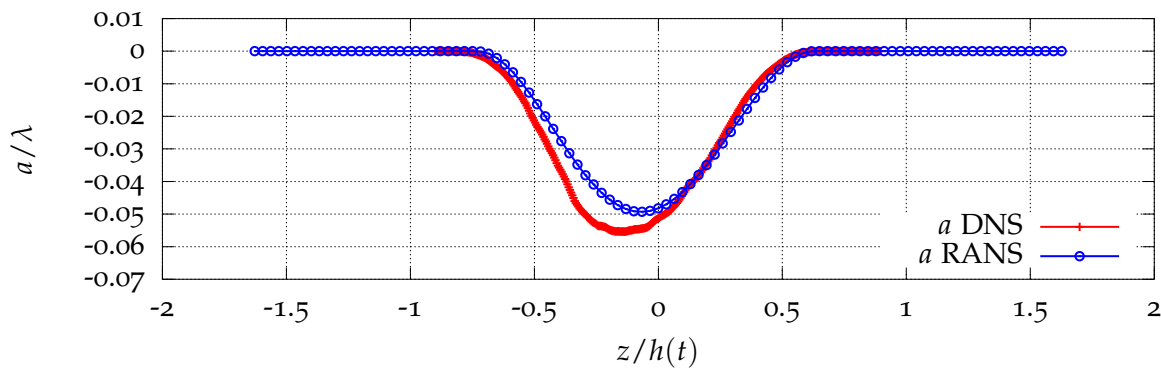
Figure 5: Comparison of DNS and RANS results for the turbulent mass-weighted velocity, a_z, for A = 0.5.

4 Modeling homogeneous variable density turbulence (HVDT)
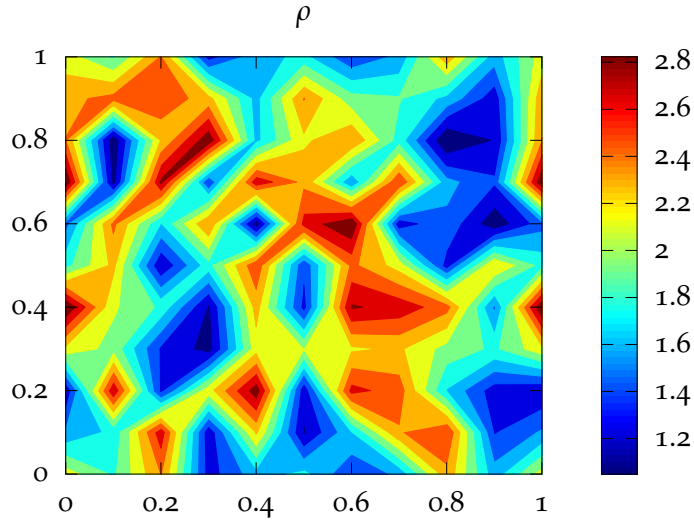
Figure 6: Illustrative example of the initial conditions for density in homogeneous variable density turbulence.

Homogeneous variable density turbulence (HVDT) is generated by modeling a homogeneous mixture of random density fluctuations in a periodic cube, e.g., as shown in figure 6. Livescu and Ristorcelli [LR07] modeled HVDT with DNS, and the results were used as another point of comparison for the development of model coefficients for the BHR3 model.

The BHR3 equations reduce to ODEs in this case. A Mathematica file was developed which integrated the BHR3 equations in time, which I used to model HVDT. The results from the current model coefficients are shown in figure 7.

Figure 7: The BHR3 model with current coefficients compared against DNS of homogeneous variable density turbulence.

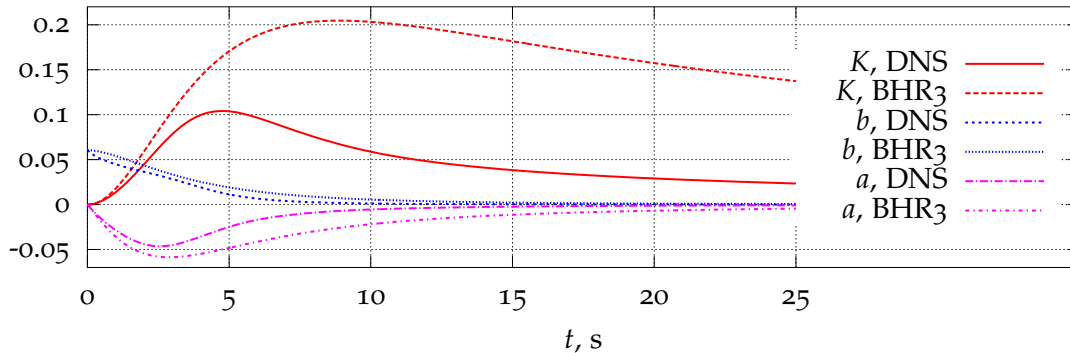| equation	new coeff.	new value	justification	old coeff.	old value
S_{diff}	C_1	1.2	KH growth rates	C_1	1.2
S_{diff}	C_2	1.77	[ML90], [KF09]	C_2	1.92
S_{diff}	C_4	1.0	RT growth rates	C_3	1.2
S_{diff}	C_3	0	—	—	—
S_{diff}	C_s	4.2	[Sch+11, p. 19]	C_s	4.2
S_{diss}	C_{1v}	0.9	KH R_{ij}, α	—	—
S_{diss}	C_{2v}	1.77	[ML90], [KF09]	—	—
S_{diss}	C_{4v}	1.31	HVDT DNS [LR07]	—	—
S_{diss}	C_{3v}	0		—	—
S_{diss}	C_{sv}	4.2		—	—
R_{ij}	C_{r3}	0.42	[Sch+11, p. 23]	C_r	0.42
R_{ij}	C_{r4}	2.6	KH R_{ij}, α	C_{r3}	1.8
R_{ij}	C_{r2}	0.6	RDT [Pop00, p. 423]	C_{r2}	0.6
R_{ij}	C_{r1}	0.3		C_{r1}	0.3
a_i	C_{ap}	0.28	RT K, a_i, b, α	—	—
a_i	C_{ar}	0		—	—
a_i	C_{au}	0		—	—
a_i	C_a	0.3	RT width	C_a	0.3
a_i	C_{a1}	2.8	RT K, a_i, b, α	C_{a1}	3.2
b	C_b	0.3	RT width	C_b	0.3
b	C_{b2}	1.8	RT K, a_i, b, α	C_{b1}	2
c_n	C_c	0.56	[Sch+11, p. 23]	C_c	0.56

Table 2: Model coefficients found to match the Rayleigh-Taylor instability and HVDT best. The old coefficients are from BHR3 before this work.

5 Model coefficients and their justification

The model coefficients developed in this work and a summary of their justification is in table 2.

5.1 Isotropic turbulence decay

The standard k-ϵ model [Pop00, p. 375-376] chooses $C_2 = 1.92$ as the isotropic turbulence decay coefficient. The first step towards improving the coefficients was to choose $C_2 = C_{2v} = 1.77$ as suggested by Mohamed and LaRue [ML90, p. 211, fig. 13] based on experimental data they compiled. More recent data summarized by Kurian and Fransson [KF09, p. 13, fig. 9(a)] suggests that C_2 increases with the grid Reynolds number, however, this may be misleading as the lower grid Reynolds number experiments had significant anisotropy [KF09, p. 9, fig. 4(a)] below a grid Reynolds number of approximately 2×10^3.

The grid Reynolds number is defined as

$$\text{Re}_M \equiv \frac{U_0 M}{\nu} \tag{5.1}$$

where U_0 is the free stream velocity, M is the mesh width, and ν is the kinematic viscosity of the fluid. The effect of M can be thought of as the initial conditions' effect. The grid Reynolds number combines the initial conditions and the fluid velocity. The dependence on the grid Reynolds number for the isotropic turbulence decay experiments may be due to the effect of the initial conditions, fluid velocity, anisotropy, or possibly a cause that was not yet considered.

The spread in the data for grid Reynolds numbers greater than about 2×10^3 suggests that $1.6 \lesssim C_2 \lesssim 1.8$
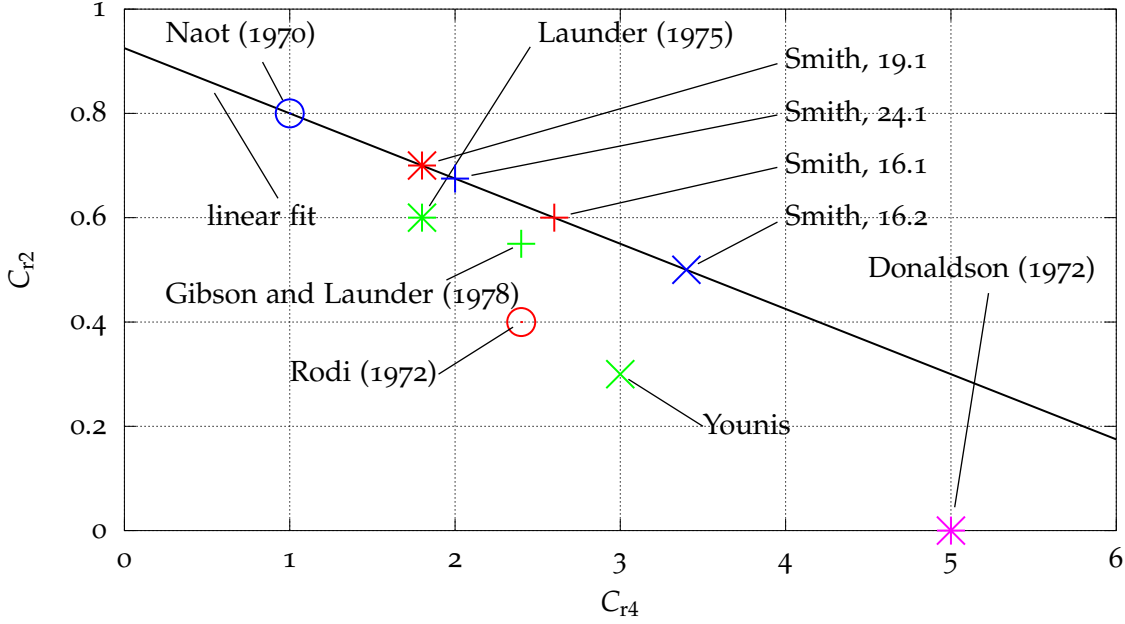
Figure 8: Proposed values of C_{r2} and C_{r4}. The BHR3 model with the coefficients on the line return results which visually match Kelvin-Helmholtz experimental data [BM90] nearly exactly [Smi12, §3.3]. The line is $C_{r2} = -0.23C_{r4} + 1$. The numbered points refer to different configurations tested. Other citations are from [Lau96, p. 268].

with most of the data clustering around $C_2 = 1.77$. Thus, choosing $C_2 = 1.77$ seems most consistent with the available experimental data.

Speziale and Bernard [SB92] prove theoretically that the isotropic decay exponent asymptotically approaches 2 as the Reynolds number increases. How high the Reynolds number needs to be for the coefficient to be near two is unclear based on the mentioned work.

5.2 Rapid distortion theory

Pope [Pop00, p. 423] notes that if C_{r2} is set to 0.6 then the isotropization-of-production model returns the correct response of rapidly distorted isotropic turbulence.

Launder [Lau96, p. 268] suggests that compatible values of C_{r2} and C_{r4} lie on a line. Smith [Smi12, §3.3] found a line that prescribes values of C_{r2} and C_{r4} as can be seen in figure 8. Using the BHR3 model with coefficients found on this line visually appear to give results which excellently match the experimental data of Bell and Mehta [BM90]. The value of C_{r4} on this line when $C_{r2} = 0.6$ is 2.6.

5.3 Kelvin-Helmholtz instability

The following coefficients fit the Kelvin-Helmholtz experiments and DNS best [Smi12, §3.3]:

$$C_1 = 1.2 \quad , \quad C_{1v} = 0.9 \quad , \quad C_{r4} = 2.6 . \tag{5.2}$$

5.4 Homogeneous variable density turbulence (HVDT)

John Schwarzkopf and I generated a wide variety of different configurations which fit the HVDT DNS data reasonably well. "Reasonably well" means that the BHR3 b was overlapping then DNS b (which is

easy to do), that the BHR3 a_z is almost overlapping or overlapping the DNS a_z, and that the BHR3 K has the same general trend as the DNS K. Perfect fit was not expected.

The coefficients with the best fit to the HVDT data were used as starting points for tweaking to fit the Rayleigh-Taylor DNS data better.

The DNS data and BHR3 model can be compared in figure 7.

The single time scale version of BHR3 had poor fit for K — the turbulent kinetic energy greatly overpredicted the DNS value. Here the RANS turbulent kinetic energy peaks with a slightly higher magnitude than the DNS data and decreases after the peak in a way qualitatively like the DNS data.

Another possible set of coefficients is similar to the coefficients in table 2, but with the following modifications:

$$C_{a1} = 1.5 \quad , \quad C_{b2} = 1.5 \quad , \quad C_{ap} = 0.40 \quad , \quad C_{4v} = 1.36 \quad , \quad C_4 = 1.12 \, . \tag{5.3}$$

Future work should consider trying these coefficients. With these coefficients the overall fit of the Reynolds stresses, turbulent kinetic energy, b, and turbulent mass-weighted density are slightly worse than with the coefficients in table 2, but not significantly so. The growth rate for the A $= 0.5$ case is slightly better ($\alpha = 0.0431$) but this can be improved in the table's coefficients.

6 Conclusions

The two-scale model is a significant improvement in the development of BHR3. With two scales Rayleigh-Taylor instabilities, the Kelvin-Helmholtz instabilities, and homogeneous variable density turbulence can be modeled reasonably accurately. The BHR3 model has been validated against a wide variety of flows for a turbulence model, and our hope is that it can be used as a general-purpose turbulence model.

Additionally, the isotropic turbulence decay coefficient was changed so that BHR3 fits the latest experimental data.

6.1 Future directions

These coefficients can be applied to Richtmyer-Meshkov instabilities to further test their applicability in general. Discrepancies can be addressed either in additional or improved turbulence models or improved model coefficients.

6.2 Acknowledgments

References

[AS90]   Malcolm J. Andrews and Dudley Brian Spalding. "A simple experiment to investigate two-dimensional mixing by Rayleigh-Taylor instability". In: *Physics of Fluids A: Fluid Dynamics* 2.6 (June 1990), pp. 922–927. ISSN: 08998213. DOI: doi:10.1063/1.857652. URL: http://pof.aip.org/resource/1/pfadeb/v2/i6/p922_s1. (Cit. on p. 5).

[BKA10]   Arindam Banerjee, Wayne N. Kraft, and Malcolm J. Andrews. "Detailed measurements of a statistically steady Rayleigh-Taylor mixing layer from small to high Atwood numbers". In: *Journal of Fluid Mechanics* 659.1 (2010), pp. 127–190. DOI: 10.1017/S0022112010002351. (Cit. on pp. 2, 5, 6).

[BM90]   James H. Bell and Rabindra D. Mehta. "Development of a two-stream mixing layer from tripped and untripped boundary layers". In: *AIAA Journal* 28.12 (1990), pp. 2034–2042. (Cit. on pp. 6, 10).

[CC06]   William H. Cabot and Andrew W. Cook. "Reynolds number effects on Rayleigh-Taylor instability with possible implications for type Ia supernovae". In: *Nature Physics* 2.8 (2006), pp. 562–568. ISSN: 1745-2473. DOI: 10.1038/nphys361. URL: http://www.nature.com/nphys/journal/v2/n8/full/nphys361.html. (Cit. on pp. 5, 6).

[CS74]   Tuncer Cebeci and A. M. O Smith. *Analysis of turbulent boundary layers*. Applied Mathematics and Mechanics 15. New York: Academic Press, June 1974. ISBN: 0121646505. (Cit. on p. 4).

[DR04]   P. G. Drazin and W. H. Reid. *Hydrodynamic Stability*. 2nd ed. Cambridge University Press, Sept. 2004. ISBN: 0521525411. (Cit. on p. 2).

[Git+08] Michael Gittings et al. "The RAGE radiation-hydrodynamic code". In: *Computational Science & Discovery* 1.1 (Nov. 2008), p. 015005. ISSN: 1749-4699. DOI: 10.1088/1749-4699/1/1/015005. URL: http://iopscience.iop.org/1749-4699/1/1/015005. (Cit. on p. 5).

[KF09]   Thomas Kurian and Jens H. M. Fransson. "Grid-generated turbulence revisited". In: *Fluid Dynamics Research* 41.2 (Apr. 2009), p. 021403. ISSN: 0169-5983, 1873-7005. DOI: 10.1088/0169-5983/41/2/021403. URL: http://iopscience.iop.org/0169-5983/41/2/021403. (Cit. on pp. 1, 9).

[Lau96]   Brain E. Launder. "An introduction to single-point closure methodology". In: *Simulation and Modeling of Turbulent Flows*. Ed. by Thomas B. Gatski, M. Yousuff Hussaini, and John L. Lumley. Oxford University Press, July 1996, pp. 243–310. ISBN: 9780195106435. (Cit. on p. 10).

[Liv+09] D. Livescu et al. "High-Reynolds number Rayleigh-Taylor turbulence". In: *Journal of Turbulence* (2009), N13. DOI: 10.1080/14685240902870448. URL: http://www.tandfonline.com/doi/abs/10.1080/14685240902870448. (Cit. on pp. 1, 4, 5).

[Liv12]   Daniel Livescu. Aug. 2012. (Cit. on pp. 6, 7).

[LR07]   Daniel Livescu and J. R. Ristorcelli. "Buoyancy-driven variable-density turbulence". In: *Journal of Fluid Mechanics* 591 (2007), pp. 43–71. DOI: 10.1017/S0022112007008270. URL: http://public.lanl.gov/livescu/frames/jfm3.pdf. (Cit. on pp. 1, 8, 9).

[ML90]   Mohsen S. Mohamed and John C. LaRue. "The decay power law in grid-generated turbulence". In: *Journal of Fluid Mechanics* 219 (1990), pp. 195–214. DOI: 10.1017/S0022112090002919. (Cit. on pp. 1, 9).

[Pop00]   Stephen B. Pope. *Turbulent Flows*. 1st ed. Cambridge University Press, Oct. 2000. ISBN: 0521598869. (Cit. on pp. 3, 4, 9, 10).

[PV05]   Thierry Poinsot and Denis Veynante. *Theoretical and numerical combustion*. R. T. Edwards, Jan. 2005. ISBN: 9781930217102. (Cit. on pp. 2, 3).

[RM94]   Michael M. Rogers and Robert D. Moser. "Direct simulation of a self-similar turbulent mixing layer". In: *Physics of Fluids* 6.2 (Feb. 1994), pp. 903–923. ISSN: 10706631. DOI: doi:10.1063/1.868325. URL: http://pof.aip.org/resource/1/phfle6/v6/i2/p903_s1. (Cit. on p. 6).

[SB92]   Charles G. Speziale and Peter S. Bernard. "The energy decay in self-preserving isotropic turbulence revisited". In: *Journal of Fluid Mechanics* 241 (1992), pp. 645–667. DOI: 10.1017/S0022112092002180. (Cit. on p. 10).

[Sch+11]   John D. Schwarzkopf et al. "Application of a second-moment closure model to mixing processes involving multicomponent miscible fluids". In: *Journal of Turbulence* (2011), N49. DOI: 10.1080/14685248.2011.633084. URL: http://www.tandfonline.com/doi/abs/10.1080/14685248.2011.633084. (Cit. on pp. 2–4, 6, 7, 9).

[Smi12]   Jeffrey Smith. *Turbulent modeling of plane mixing layer*. Tech. rep. Los Alamos National Lab, Aug. 2012. (Cit. on pp. 6, 10).

7   Appendix A: Input deck

```
1
2   ! Modified from base case A=0.04 TAMU water channel data
3
4   !================================================================================
5   ! CONTROL
6   !================================================================================
7   secmax = 396000    ! How long run should go (in secs)
8   pname = "rt2s"   ! all output files have this prefix
9
10  test_pname='rt11_1v'    ! 2d R-T
11  userparms(1)=1.         ! rho-lo
12  userparms(2)=3.         ! rho-hi
13  userparms(3)=1.e4       ! rho*cv
14  userparms(4)=2000.      ! tev0
15  userparms(5)=0.4        ! GAMMA-1
16
17  mincellpe = 0      ! For parallel runs these two entries determine the min and
18  maxcellpe = 0      ! max number of cells on each processor.  0 turns it off
19  ncmax = 50000000   ! Maximum number of cycles (timesteps) to run
20  secmax = 27000
21  tmax = 2.6         ! Maximum time in simulation time units
22  tedit = 5.e-1      ! How often to print status information and restart dumps
23  ncedit = 1000      ! If not 0 how many cycles between status and restart dumps
24  modcyc = 1000      ! Status dumps only
25
26  kread = -1         ! Does nothing at -1, other #'s determine cycle to restart
27  uselast = .true.   ! If restart dumps exists in this director, use the last one
28                     ! Note: if this happens some initialization parameters
29                     ! set later are skipped.
30  shortmodcyc = 10        ! Prints a short status message every cycle
31
32
33  !================================================================================
34  ! Hydro
35  !================================================================================
36  numrho = 4
37  hydro_version = 2
38  interface_option = 0
39
40
41  ! TURBULENCE MIX
42  !S0_max = 1.0
43   do_mix = .true.              ! Turn on/off BHR
44   mix_model = 'BHR-3'
45   mix_t_start=0.               ! Determine when model is turned on
46   mix_t_end=10.e8              ! Determine when model is turned off
47   turb_scale_0 = 0.1000        ! Determine initial length scale
48   turb_ske_0 = 0.25            ! Determine initial value for ke
49   const_scale = .false.        ! Use a regular L-transport equation
50   use_mixscale =.true.
51   mix_b_cutoff = 1.0e-20
52   mix_numrho = 4
53   use_mixvisc_scale = .true.! uses both S eqns (must be false for BHR-2)
54   num_mixmat=2                 ! Number of materials to be mixed
55   mixmat(1)=1,2                ! Allow both materials to mix
56   use_Rij_diff_coef=.true. ! .false. means it uses turbulent viscosity
```

```
57
58  !==============================================================================
59  ! Coefficients for students to alter
60  !==============================================================================
61  ! coefficients that affect variable density RT
62    mix_ca1  = 2.80 ! fit this
63    mix_cb2  = 1.80 ! fit this
64    mix_cap  = 0.28 ! fit this
65    mix_c4v  = 1.31 ! adjust to fit HVDT DNS data
66    mix_c4   = 1.00 ! adjust to get correct growth rate
67
68    mix_c_a  = 0.30 ! adjust to get correct widths
69    mix_c_b  = 0.30 ! adjust to get correct widths
70    mix_c_c  = 0.56
71    mix_cr1  = 0.3
72    mix_cau  = 0.0
73    mix_car  = 0.0
74
75  ! coefficients that affect single phase KH
76    mix_c1   = 1.2
77    mix_c1v  = 0.9  ! set from KH
78    mix_cr2  = 0.6  ! do not change, RDT, see Pope p. 423
79    mix_cr3  = 0.42
80
81  ! coefficients that affect both
82    mix_cr4  = 2.6  ! set from KH
83    mix_c2   = 1.77 ! do not change
84    mix_c2v  = 1.77 ! do not change
85    mix_c_s  = 4.2
86    mix_c_sv = 4.2
87
88  ! Additional coefs
89    mix_c3   = 0.0  ! leave at zero
90    mix_c3v  = 0.0  ! leave at zero
91  !==============================================================================
92  ! PLOTS
93  !==============================================================================
94
95  !mix_plts = .true.
96  !mix_plts_ncedit = 250
97  !mix_plts_xmn = 0.0
98  !mix_plts_xmx = 0.25
99  !mix_plts_ymn =-80.0
100 !mix_plts_ymx = 80.0
101 !mix_plts_ncstart = 1
102 ! mix_plts_tmzdir = 'y'
103 ! mix_plts_tmzmat = 1
104 !mix_vfedge=0.01
105
106 ! pop
107 use_int_method_2=.false.
108 use_tracers=.false.
109 num_mixreg=2                       ! Number of material regions to be mixed (can be greater
        than num_mixmat)
110 mixmat_order(1)=1,2    ! User must specify order of materials from r=0 to rmax
111 dopop=.true.
112 pop_dt=5.0e-2
113 dodmpxdt=.true.
114 !pop_cycle=100
```

```
115  npop_prob=1
116  pop_prob(1)='mass'
117  npop_matl=6
118  !npop_matl=1
119  pop_matl(1)='tev'
120  pop_matl(2)='rho'
121  pop_matl(3)='sie'
122  pop_matl(4)='mix_2'
123  pop_matl(5)='intpos_2_lo'
124  pop_matl(6)='intpos_2_hi'
125  npop_mesh=20
126  pop_mesh(1)='tev'
127  pop_mesh(2)='rho'
128  pop_mesh(3)='c01'
129  pop_mesh(4)='c02'
130  pop_mesh(5)='ten'
131  pop_mesh(6)='a_1'
132  pop_mesh(7)='mxb'
133  pop_mesh(8)='tsc'
134  pop_mesh(9)='ydt'
135  pop_mesh(10)='prs'
136  pop_mesh(11)='snd'
137  pop_mesh(12)='a_2'
138  !JDS added the following pop_mesh
139  pop_mesh(13)='Rnn'
140  pop_mesh(14)='RS1'
141  pop_mesh(15)='RS2'
142  pop_mesh(16)='RS3'
143  pop_mesh(17)='RS4'
144  pop_mesh(18)='RS5'
145  pop_mesh(19)='RS6'
146  pop_mesh(20)='tvs'
147
148
149  !=============================================================================
150  ! SETUP
151  !=============================================================================
152  ! numfine = 7           ! See RAGE page
153  dxset = 0.125        ! size of zones in x and y (must be equal)
154  dyset = 0.125
155  imxset = 2           ! How many coarsest zones in x- and y-direction
156  jmxset = 2400
157  xzero =  0.0         ! minimum x and y values
158  yzero = -150.
159
160  ! resolutions
161  !!!!! l0 = 0.25
162  ! l1 = 0.125          ! 1000 micron
163  !  2    0.0625
164  !  3    0.03125
165  !  4    0.015625      ! 156 micron
166  !  5    0.0078125
167  !  6    0.00390625
168  !  7    0.001953125   ! 19 micron
169
170  !sizemat(1) = 2*0.001953125        ! Base level of zones for this material
171  !sizebnd(1) = 2*0.001953125          ! How fine to go at interfaces with other materials
172  sizerho(1) = 2*0.5          ! adapt if delta-rho is bigger than this
```

```
173   fvolpct = 0.00005            ! Change in fractional volume for use in determining if near
          interf
174
175   !==============================================================================
176   ! MATERIALS
177   !==============================================================================
178   keos = 0                     ! keos = 0 means analytic (gamma-law) EOS
179   nummat = 2                   ! How many distinct materials are there?
180
181   ! ideal gases can have pressure and temperature equilibrium if
182   ! (g1-1)*rho1*cv1*T = (g2-1)*rho2*cv2*T; ie. rho*cv = const
183
184   matdef(1,1) = 0.0            ! I forget
185   matdef(16,1) = 0.4          ! gamma - 1.0
186   matdef(30,1) = 10000.0       ! C_v for material
187
188   matdef(1,2) = 0.0
189   matdef(16,2) = 0.4          ! gamma - 1.0
190   matdef(30,2) = 3333.333333
191
192
193   !tevbca=9.93875
194   !tevbcb=10.1225
195
196
197   !==============================================================================
198   ! REGIONS
199   !==============================================================================
200   numreg = 2
201
202   matreg(1) = 1               ! ambient, low-density material
203   rhoreg(1) = 1.0
204   tevreg(1) = 2000.
205
206   matreg(2) = 2               ! overlying higher-density material
207   rhoreg(2) = 3.0      !need to change matdef(30,2) also need to change rho-hi above
208   tevreg(2) = 2000.
209
210   typreg(2) = 13    ! region two is above the interface calculated
211   fitreg(2) = 1
212   loreg(2) = 2
213   hireg(2) = 2
214   coefreg(1,2) = 0.0000000  ! .01  Interface perturbation (amplitude)
215   coefreg(2,2) = 1.0 ! Box size (wavelength)
216   coefreg(3,2) = 0.0    ! No phase offset to yint= c1*cos(2*pi*x/c2)
217
218   ! reference instructions for doing the linear stability problem
219   !  To properly run a Rayleigh-Taylor incompressible problem, one has to set the
220   !  initial conditions to values that are self-similar.  Thus both the interface
221   !  position and velocity should be perturbed, and v0 = gamma*z0, where gamma**2 = k*g*A
222   !  with k = (2*pi/L), g= gravity, and A=Atwood# = (rhohi-rholo)/(rhohi+rholo)
223   !  if box is size one, k = 2*pi.  If g  = 100/2pi =aprox= 15.915, then gamma**2 = 10*sqrt(
          A)
224   !  if Atwood =  0.36 (2.125:1), then gamma = 6.0
225   !  AND, one wants the interface perturbation to be small (imperceptible) wrt box size
226
227   !  lambda     k       g          A       gamma    a0      t     amr lev   yanaly   ycalc
228   !  ------    ----  ---------   -----   ------    ----    ----   -------   ------   -----
229   !   1.0     2pi    100/2pi     .36       6       .01     .038             .023
```

```
230  !   1.0     2pi    10000/2pi    .36       60       .025   .019     5       .103      .06-.08
231
232  ! This is the run in the repository.
233  !   1.0     2pi    10000/2pi    .36       60       .025   .019     3       .103
234
235  rttype = 3              ! prestress and set velocities to self-similar initial conditions
236  rt_num=1
237  rt_coefa(1)=0.0   !0.00      ! v0 = gamma*z0, and coefreg(1,2) = 0.01
238  rt_coefb(1)=1.0   ! so k = 2*pi/1.0  .  If box is not unit sized, rt_coefb=size
239
240
241  !===============================================================================
242  ! Gravity/ Prestress
243  !===============================================================================
244  grav_y = -1000.00                    ! cm/s**2  ==> growthrate=60 /sec
245  do_grav_prestress = .false.      ! neither 1d-x or 2-d spherical
246  !
        !!!!!!!!!!!!!!!!!!!!!!!!!!!!!!!!!!!!!!!!!!!!!!!!!!!!!!!!!!!!!!!!!!!!!!!!!!!!!!!!!!!!!!!!!!!!!!!!!!!!!!!!!!

247
248  !ncmax = 15  ! Maximum number of cycles (timesteps) to run
249  sizemat(1)=2*0.0625
250  sizebnd(1)=2*0.0625
251  !kread = 10         ! Does nothing at -1, other #'s determine cycle to restart
```

8 Appendix B: Post-processing script

```
1   clear all
2   close all
3   more off
4
5   plotz = true;
6
7   rho_min = 1;
8   rho_max = 3;
9
10  locspec = 0.01;
11
12  # 1 --- z/h(t)
13  # 2 --- tke
14  # 3 --- a
15  # 4 --- mxb
16  # 5 --- R11
17  # 6 --- R33
18  # 7 --- rho (does not exist for DNS?)
19
20  # read in the DNS data
21  load -ascii "dns_data.csv"
22
23  zoht_dns = dns_data(:, 1);
24  tke_dns = dns_data(:, 2);
25  a_dns = dns_data(:, 3);
26  mxb_dns = dns_data(:, 4);
27  R11_dns = dns_data(:, 5);
28  R33_dns = dns_data(:, 6);
29
30  tke_smo = supsmu(zoht_dns, tke_dns);
31  a_smo = supsmu(zoht_dns, a_dns);
32  mxb_smo = supsmu(zoht_dns, mxb_dns);
33  R11_smo = supsmu(zoht_dns, R11_dns);
34  R33_smo = supsmu(zoht_dns, R33_dns);
35
36  tke_smoindx = find(tke_smo > (locspec * (max(tke_smo) - min(tke_smo)) + min(tke_smo)));
37  mxb_smoindx = find(mxb_smo > (locspec * (max(mxb_smo) - min(mxb_smo)) + min(mxb_smo)));
38  a_smoindx = find(a_smo > (locspec * (max(a_smo) - min(a_smo)) + min(a_smo)));
39
40  tke_smoindxmin = min(tke_smoindx);
41  mxb_smoindxmin = min(mxb_smoindx);
42  a_smoindxmin = min(a_smoindx);
43
44  tke_smoindxmax = max(tke_smoindx);
45  mxb_smoindxmax = max(mxb_smoindx);
46  a_smoindxmax = max(a_smoindx);
47
48  if plotz == true
49      figure(1)
50      plot(zoht_dns, tke_dns, 'b')
51      hold on
52      plot(zoht_dns, tke_smo, 'r')
53
54      figure(2)
55      plot(zoht_dns, mxb_dns, 'b')
56      hold on
```

```
57      plot(zoht_dns, mxb_smo, 'r')
58
59      figure(3)
60      plot(zoht_dns, a_dns, 'b')
61      hold on
62      plot(zoht_dns, a_smo, 'r')
63
64      figure(4)
65      plot(zoht_dns, R11_dns, 'b')
66      hold on
67      plot(zoht_dns, R11_smo, 'r')
68
69      figure(5)
70      plot(zoht_dns, R33_dns, 'b')
71      hold on
72      plot(zoht_dns, R33_smo, 'r')
73  end
74
75  for i = [45]
76      filename = ['data' num2str(i) '.csv']
77
78      # read in the RAGE data
79      copyfile(filename, "tempcsv.csv");
80      load -ascii "tempcsv.csv"
81      unlink("tempcsv.csv");
82
83      z = tempcsv(:, 1);
84      tke = tempcsv(:, 2);
85      a = tempcsv(:, 3);
86      mxb = tempcsv(:, 4);
87      R11 = tempcsv(:, 5);
88      R33 = tempcsv(:, 6);
89      rho = tempcsv(:, 7);
90      rho_older = tempcsv(:, 8);
91
92      # scale the RAGE data
93      f_v = (rho - rho_min) / (rho_max - rho_min);
94
95      integrand = f_v .* (1 - f_v);
96
97      ht = 6 * trapz(z, integrand);
98
99      scale = ht^2 / (ht / 500);
100
101     zoht = z / ht;
102     tke = 1e16 * tke / scale;
103     a = a / sqrt(scale);
104     mxb = mxb;
105     R11 = 1e16 * R11 / scale;
106     R33 = 1e16 * R33 / scale;
107
108     #matout = [zoht tke a mxb R11 R33 rho rho_older];
109     #size(matout)
110
111     #unlink("output.csv");
112     #save -ascii "output.csv" matout
113
114     # earlier (t = 2.2 s) mix width
115     f_v = (rho_older - rho_min) / (rho_max - rho_min);
```

```
116
117     integrand = f_v .* (1 - f_v);
118
119     ht_older = 6 * trapz(z, integrand);
120
121     #t_new = 2.0;
122     #t_older = 1.7;
123     #t_new = 2.5;
124     #t_older = 2.2;
125
126     t_new = 2.1;
127     t_older = 2.0;
128
129     # calculate growth rate
130
131     alpha_dns = 0.0416; # for A = 0.5 (see p. 22 of Schwarzkopf, et al. (2011))
132     alpha = ((sqrt(ht) - sqrt(ht_older)) / (sqrt(500) * (t_new - t_older))) ^ 2;
133
134     errvec = [];
135
136     % peak-to-peak
137     errvec(1) = abs(max(abs(tke)) - max(abs(tke_smo))) / abs(max(abs(tke_smo)) + max(abs(
            tke)));
138     errvec(2) = abs(max(abs(mxb)) - max(abs(mxb_smo))) / abs(max(abs(mxb_smo)) + max(abs(
            mxb)));
139     errvec(3) = abs(max(abs(a)) - max(abs(a_smo))) / abs(max(abs(a_smo)) + max(abs(a)));
140
141     % integral
142     errvec(4) = abs(trapz(zoht, tke) - trapz(zoht_dns, tke_smo)) / abs(trapz(zoht, tke) +
            trapz(zoht_dns, tke_smo));
143     errvec(5) = abs(trapz(zoht, mxb) - trapz(zoht_dns, mxb_smo)) / abs(trapz(zoht, mxb) +
            trapz(zoht_dns, mxb_smo));
144     errvec(6) = abs(trapz(zoht, a) - trapz(zoht_dns, a_smo)) / abs(trapz(zoht, a) + trapz(
            zoht_dns, a_smo));
145
146     % calculate the indices of the transition locations
147     tkeindx = find(tke > (locspec * (max(tke) - min(tke)) + min(tke)));
148     mxbindx = find(mxb > (locspec * (max(mxb) - min(mxb)) + min(mxb)));
149     aindx = find(a > (locspec * (max(a) - min(a)) + min(a)));
150
151     tkeindxmin = min(tkeindx);
152     mxbindxmin = min(mxbindx);
153     aindxmin = min(aindx);
154
155     tkeindxmax = max(tkeindx);
156     mxbindxmax = max(mxbindx);
157     aindxmax = max(aindx);
158
159     % width
160     errvec(7) = abs(1 - (zoht(tkeindxmax) - zoht(tkeindxmin)));
161     errvec(8) = abs(1 - (zoht(mxbindxmax) - zoht(mxbindxmin)));
162     errvec(9) = abs(1 - (zoht(tkeindxmax) - zoht(tkeindxmin)));
163
164     % growth rate
165     errvec(10) = 5 * abs(alpha_dns - alpha) / (abs(alpha_dns) + abs(alpha));
166     alpha
167
168     [i, sum(errvec)]
169     %errvec
```

```
170
171     if plotz == true
172        figure(1)
173        plot(zoht, tke, '0')
174        figure(2)
175        plot(zoht, mxb, '0')
176        figure(3)
177        plot(zoht, a, '0')
178        figure(4)
179        plot(zoht, R11, '0')
180        figure(5)
181        plot(zoht, R33, '0')
182     end
183  end
184
185  if plotz == true
186     figure(1)
187     title('TKE')
188     xlabel('z / h(t)')
189     ylabel('K / \lambda^2')
190     #print -dpng K.png
191
192     figure(2)
193     title('b')
194     xlabel('z / h(t)')
195     ylabel('b')
196     #print -dpng b.png
197
198     figure(3)
199     title('a')
200     xlabel('z / h(t)')
201     ylabel('a / \lambda')
202     #print -dpng a.png
203
204     figure(4)
205     title('R11')
206     xlabel('z / h(t)')
207     ylabel('R11 / \lambda^2')
208     #print -dpng R11.png
209
210     figure(5)
211     title('R33')
212     xlabel('z / h(t)')
213     ylabel('R33 / \lambda^2')
214     #print -dpng R33.png
215
216     hold off
217  end
```